PNAS PLUS

Functional hierarchy underlies preferential connectivity disturbances in schizophrenia

Genevieve J. Yang[a,b,c], John D. Murray[a,d], Xiao-Jing Wang[d,e], David C. Glahn[a,f], Godfrey D. Pearlson[a,f,g], Grega Repovs[h], John H. Krystal[a,c,g], and Alan Anticevic[a,b,c,f,i,1]

[a]Department of Psychiatry, Yale University School of Medicine, New Haven, CT 06511; [b]Interdepartmental Neuroscience Program, Department of Neurobiology, Yale University, New Haven, CT 06520; [c]Abraham Ribicoff Research Facilities, Department of Psychiatry, Connecticut Mental Health Center, New Haven, CT 06519; [d]Center for Neural Science, New York University (NYU), New York, NY 06510; [e]New York University-East China Normal University Institute of Brain and Cognitive Science, Department of Neural Science, NYU Shanghai, Pudong, 200122 Shanghai, China; [f]Olin Neuropsychiatry Research Center, Institute of Living, Hartford Hospital, CT 06106; [g]Department of Neurobiology, Yale University School of Medicine, New Haven, CT 06520; [h]Department of Psychology, University of Ljubljana, 1000 Ljubljana, Slovenia; and [i]Department of Psychology, Yale University, CT 06520

Edited by Marcus E. Raichle, Washington University in St. Louis, St. Louis, MO, and approved November 20, 2015 (received for review April 29, 2015)

Schizophrenia may involve an elevated excitation/inhibition (E/I) ratio in cortical microcircuits. It remains unknown how this regulatory disturbance maps onto neuroimaging findings. To address this issue, we implemented E/I perturbations within a neural model of large-scale functional connectivity, which predicted hyperconnectivity following E/I elevation. To test predictions, we examined resting-state functional MRI in 161 schizophrenia patients and 164 healthy subjects. As predicted, patients exhibited elevated functional connectivity that correlated with symptom levels, and was most prominent in association cortices, such as the fronto-parietal control network. This pattern was absent in patients with bipolar disorder (n = 73). To account for the pattern observed in schizophrenia, we integrated neurobiologically plausible, hierarchical differences in association vs. sensory recurrent neuronal dynamics into our model. This in silico architecture revealed preferential vulnerability of association networks to E/I imbalance, which we verified empirically. Reported effects implicate widespread microcircuit E/I imbalance as a parsimonious mechanism for emergent inhomogeneous dysconnectivity in schizophrenia.

functional connectivity | schizophrenia | computational modeling

Schizophrenia (SCZ) is a disabling psychiatric disease associated with widespread neural disturbances. These involve abnormal neurodevelopment (1–3), neurochemistry (4–7), neuronal gene expression (8–11), and altered microscale neural architecture (2). Such deficits are hypothesized to impact excitation-inhibition (E/I) balance in cortical microcircuits (12). Clinically, SCZ patients display a wide range of symptoms, including delusions, hallucinations (13, 14), higher-level cognitive deficits (15, 16), and lower-level sensory alterations (17). This display is consistent with a widespread neuropathology (18), such as the E/I imbalance suggested by the NMDA receptor (NMDAR) hypofunction model (19–21). However, emerging resting-state functional magnetic resonance imaging (rs-fMRI) studies implicate more network-specific abnormalities in SCZ. Typically, these alterations are localized to higher-order association regions, such as the fronto-parietal control network (FPCN) (18, 22) and the default mode network (DMN) (23, 24), with corresponding disturbances in thalamo-cortical circuits connecting to association regions (25, 26). It remains unknown how to reconcile widespread cellular-level neuropathology in SCZ (20, 21, 27, 28) with preferential association network disruptions (29, 30).

Currently a tension exists between two competing frameworks: global versus localized neural dysfunction in SCZ. Association network alterations in SCZ, identified via neuroimaging, may arise from a localized dysfunction (3, 9, 31, 32). Alternatively, they may represent preferential abnormalities arising emergently from a nonspecific global microcircuit disruption (20, 33). Mechanistically, an emergent preferential effect could occur because of intrinsic differences between cortical areas in the healthy brain, leading to differential vulnerability toward a widespread homogenous neuropathology. For example, histological studies of healthy primate brains show interregional variation in cortical cytoarchitectonics (34–38). Additional studies reveal differences in microscale organization and activity timescales for neuronal populations in higher-order association cortex compared with lower-order sensory regions (38–40). However, these well-established neuroanatomical and neurophysiological hierarchies have yet to be systematically applied to inform network-level neuroimaging disturbances in SCZ. In this study, we examined the neuroimaging consequences of cortical hierarchy as defined by neurophysiological criteria (i.e., functional) rather than anatomical or structural criteria.

One way to link cellular-level neuropathology hypotheses with neuroimaging is via biophysically based computational models (18, 41). Although these models have been applied to SCZ, none have integrated cortical hierarchy into their architecture. Here we initially implemented elevated E/I ratio within our well-validated computational model of resting-state neural activity (18, 42, 43) without assuming physiological differences between brain regions, but maintaining anatomical differences. The model predicted widespread elevated functional connectivity as a consequence of elevated E/I ratio. In turn, we tested this connectivity prediction across 161 SCZ patients and 164 matched healthy comparison subjects (HCS). However, we discovered an inhomogeneous spatial

Significance

Schizophrenia is linked to widespread neuronal-level changes causing cortical excitation-inhibition imbalance. However, functional neuroimaging reveals preferential association network dysconnectivity. Therefore, a tension exists between two competing frameworks: global versus localized neural dysfunction in schizophrenia. To link these levels of analysis, this study initially simulated cellular-level glutamatergic deficits, generating network-level predictions of cortical imbalance. Schizophrenia results revealed widespread hyperconnectivity in line with model predictions, yet effects were most profound within association networks. These clinical effects were computationally captured by considering a pre-existing functional cortical hierarchy between association and sensory regions. This study reveals that widespread cellular deficits in schizophrenia can give rise to network-preferential disruptions observed in neuroimaging as an emergent property of pre-existing functional differences between cortical areas.

Author contributions: G.J.Y., J.D.M., and A.A. designed research; G.J.Y. and A.A. performed research; G.J.Y., J.D.M., X.-J.W., G.R., and A.A. contributed new reagents/analytic tools; G.J.Y. analyzed data; G.J.Y., J.D.M., X.-J.W., D.C.G., G.D.P., G.R., J.H.K., and A.A. wrote the paper; and D.C.G. and G.D.P. acquired data.

The authors declare no conflict of interest.

This article is a PNAS Direct Submission.

[1]To whom correspondence should be addressed. Email: alan.anticevic@yale.edu.

This article contains supporting information online at www.pnas.org/lookup/suppl/doi:10.1073/pnas.1508436113/-/DCSupplemental.

pattern of elevated connectivity in SCZ generally centered on association cortices.

To capture the observed inhomogeneity, we hypothesized that pre-existing intrinsic regional differences between association and lower-order cortical regions may give rise to preferential network-level vulnerability to elevated E/I. Guided by primate studies examining activity timescale differences across the cortical hierarchy (39, 44), we incorporated physiological differentiation across cortical regions in the model. Specifically, we tested whether pre-existing stronger recurrent excitation in "association" networks (39, 40) would preferentially increase their functional connectivity in response to globally elevated E/I. Indeed, modeling simulations predicted preferential effects of E/I elevation in association networks, which could not be explained by structural connectivity differences alone.

Finally, we empirically tested all model-derived predictions by examining network-specific disruptions in SCZ. To investigate diagnostic specificity of SCZ effects, we examined an independent sample of bipolar disorder (BD) patients ($n = 73$) that did not follow model-derived predictions. These results collectively support a parsimonious theoretical framework whereby emergent preferential association network disruptions in SCZ can arise from widespread and nonspecific E/I elevations at the microcircuit level. This computational psychiatry study (45) illustrates the productive interplay between biologically grounded modeling and clinical effects, which may inform refinement of neuroimaging markers and ultimately rational development of treatments for SCZ.

Results

Functional Connectivity Is Increased in SCZ and in Simulations of Disinhibited Brain Networks. We first examined predictions of altered microcircuit E/I balance using a validated biophysically based computational model of resting-state brain activity (Fig. 1*A*) (18, 42, 43) (see *Experimental Procedures* and *SI Appendix* for model implementation detail). The model is comprised of 66 nodes representing distinct neuronal populations simulated by mean-field dynamics (46) and converted to blood oxygen level-dependent (BOLD) signals using the Balloon-Windkessel model (47). Nodes are comprised of local E and I neuronal pools. The E pools are coupled via long-range excitatory projections. The long-range connection strengths are set by interareal anatomical connectivity derived from diffusion-weighted imaging in humans (48). Using this architecture, we examined well-established SCZ hypotheses that implicate elevated E/I in cortical microcircuits, potentially induced by NMDAR hypofunction (17, 18, 41, 49–51).

We first studied an "undifferentiated" model in which all nodes had uniform strengths of local recurrent excitation. Parameters corresponding to a "healthy" regime (balanced E/I at each node) produced resting-state E-cell population firing rates of ∼3 Hz (42). To test the consequences of elevated E/I on model-derived functional connectivity, we manipulated four key parameters: weight of local self-excitation (E-E weight) within nodes, local feedback inhibition (E-I weight) within nodes, long-range, global coupling weight (G) between nodes, and local noise amplitude (σ) of background input. We computed functional connectivity across all 66 nodes using simulated BOLD signals via our global brain connectivity (GBC) approach, which was validated across a number of clinical studies (52) (*SI Appendix*). Of note, here we used covariance (as opposed to correlation) to compute functional connectivity, given recent simulation studies (53) and empirical reports (18) showing that variance normalization can fundamentally obscure clinical interpretations (*SI Appendix*).

In response to increased E-E weight or G, all 66 nodes exhibited elevated global functional connectivity (i.e., GBC) (Fig. 1 *B* and *D*). Similarly, by reducing feedback inhibition in the model (i.e., reduction in the E-I weight), we again observed elevated model-derived GBC (Fig. 1*C*), consistent with SCZ hypotheses implicating abnormal feedback inhibition (54–57). In contrast, elevating σ (noise) did not impact GBC to the same extent (Fig. 1*E*).

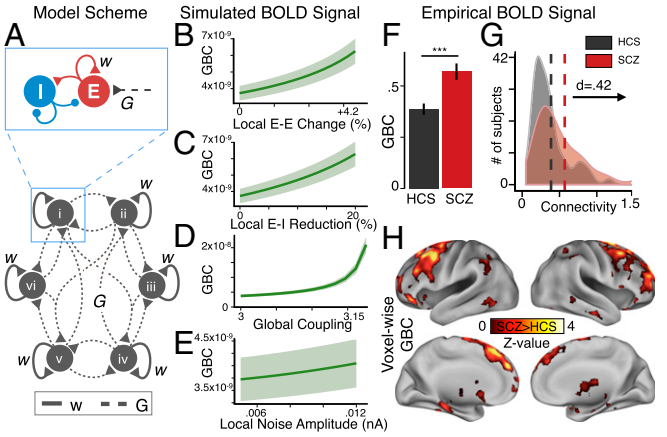

Fig. 1. Functional connectivity increases as a generic effect of elevated E/I ratio. (*A*) Schematic of computational model used to generate BOLD signals under conditions of increased E/I ratio (i.e., disinhibition). Illustration depicts six nodes for visual simplicity; full model has 66 nodes. (*B–E*) Mean covariance of each node with all other nodes, yielding GBC, as a function of increasing E-E weight (*B*), reducing E-I weight (i.e., attenuating feedback inhibition) (*C*), increasing G (*D*), or noise amplitude (*E*). Shading represents the SD of GBC values across four separate simulations with different starting random noise. (*F*) To test model predictions, GBC was computed from an a priori defined parcellation of empirical fMRI data using identical calculations as for the model (*SI Appendix*). The bar plot shows mean GBC for SCZ vs. HCS [$t(287) = 3.8$, $P < 2 \times 10^{-4}$]. (*G*) Distribution of GBC values for each group (SCZ, red; HCS, black/gray). Vertical lines represent group mean values, showing a significant rightward shift for SCZ vs. HCS [Cohen's $d = 0.42$]. (*H*) Type I error-corrected voxel-wise GBC map, revealing distributed increases in GBC for SCZ, particularly in prefrontal and thalamic regions (see *SI Appendix*, Table S3 for full list of regions; see Fig. 2 for network overlap calculation). Error bars mark ±1 SEM; ***$P < 0.001$; d = Cohen's d effect size. GBC in the model is in arbitrary units.

To empirically test model-derived predictions, we extracted BOLD signal from 161 SCZ and 164 HCS (*SI Appendix*, Table S1) using an a priori functional network-based parcellation comprised of 89 areas (58). We computed mean GBC over all 89 areas in each subject, exactly as was done for the model-generated BOLD signals above (*SI Appendix*). Consistent with model predictions for elevated E/I, we found elevated GBC across gray matter in SCZ compared with HCS [$t(287) = 3.8$, $P < 2 \times 10^{-4}$, Cohen's $d = 0.42$] (Fig. 1 *F* and *G*). In turn, we examined an independent sample of 73 BD patients and matched HCS ($n = 56$) to test if effects were specific to SCZ (see *SI Appendix*, Table S2 for demographics). BD patients did not differ from their respective matched controls [$t(95) = 0.99$, $P = 0.33$, n.s.].

Furthermore, SCZ effects were not explained by smoking status or head motion (*SI Appendix*, Fig. S1 *B* and *C*). We identified a positive relationship with medication dose (*SI Appendix*, Fig. S1*A*; see also *Discussion*). SCZ whole-brain GBC remained elevated irrespective of global signal removal ($P = 0.0015$) (*SI Appendix*, Fig. S2).

Finally, to characterize the location of significantly elevated connectivity, we computed a data-driven map for SCZ relative to HCS (Fig. 1*H*), which revealed elevated GBC across distributed cortical areas, including the thalamus and cerebellum (see *SI Appendix*, Table S3 for region coordinates and statistics surviving whole-brain type I error correction; see *SI Appendix*, Fig. S3 for cerebellum findings).

Characterizing Spatial Patterns of Connectivity Changes in SCZ. Consistent with qualitative observations (Fig. 1*H*), voxels showing elevated whole-brain connectivity in SCZ colocalized to the

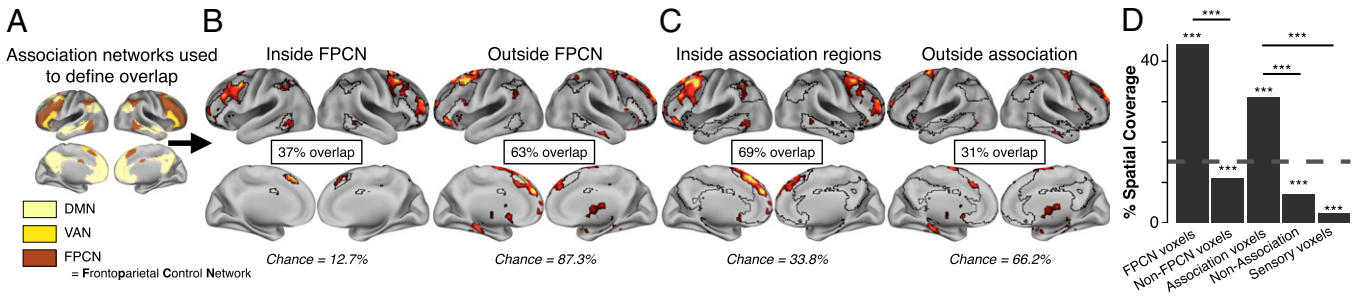

Fig. 2. Quantifying overlap between increased whole-brain connectivity in SCZ and independently defined association regions. (*A*) Using a priori defined, network-based parcellations (58, 101), we defined areal boundaries for the FPCN, and for the association cortex comprised of the FPCN, DMN, and VAN. (*B*) After down-sampling images to 10-mm voxels, to attenuate spatial correlations, 37% of areas showing elevated SCZ connectivity (Fig. 1*H*) overlapped with the FPCN (12.7% of total down-sampled gray matter voxels belong to the FPCN). In contrast, for the outside FPCN region, defined as all cortical gray matter not belonging to FPCN, there was far less overlap with regions of elevated SCZ connectivity (63%) than expected by chance (87.3%). (*C*) We repeated analyses using all association networks (FPCN, DMN, and VAN), again showing preferential colocalization of elevated SCZ connectivity with association regions. Again, the outside association region was defined as all cortical gray matter not belonging to the association region comprised of the FPCN, DMN, and VAN. An additional control analysis was computed using the combined sensory networks (*SI Appendix*, Fig. S11). (*D*) The significance above each bar represents the result from binomial tests computed for *B* and *C* and for sensory networks in *SI Appendix*, Fig. S11, comparing the expected percentage of significant voxels with the observed percentage of total significant voxels lying within each region (inside FPCN, outside FPCN, inside association, outside association, sensory networks). The percent spatial coverage plotted represents the total number of significant voxels in a region, divided by the total number of voxels for that region. The significance between bars marks difference between proportions, comparing spatial coverage within the FPCN (or association cortex) with spatial coverage outside, or comparing spatial coverage in association regions vs. spatial coverage in sensory regions. The dashed line marks the spatial coverage of all gray matter voxels by significant voxels (Fig. 1*H*). ***$P < 0.001$. Brain images are for visualization purposes only and have not been down-sampled. All reported statistics are computed on images that have been down-sampled to 10-mm voxels. Results remain unchanged without down-sampling (*SI Appendix*, Fig. S11).

FPCN (binomial test for proportions, $P < 0.001$) (Fig. 2 *B* and *D*]. The same pattern remained evident across association networks [i.e., FPCN, DMN, and ventral attention network (VAN)] (Fig. 2). A complementary analysis of elevated SCZ connectivity revealed significantly different proportions with respect to spatial coverage of the FPCN (or association networks) vs. spatial coverage elsewhere (test for difference in proportions, $P < 0.001$ for FPCN vs. not FPCN, and for association vs. not association regions) (Fig. 2*D*).

Connectivity Between Association Networks Is Increased in SCZ and Correlates with Symptoms. We identified elevated GBC preferentially within association networks and particularly within the FPCN in SCZ. However, the FPCN may also exhibit altered connectivity with other large-scale networks in SCZ, particularly the DMN, as suggested by recent qualitative reports (22). We examined this possibility by computing BOLD signal covariance between the FPCN and other networks (Fig. 3 *A*–*F*) (*SI Appendix*). Specifically, we quantified covariance between the FPCN and DMN (Fig. 3 *A*–*C*). As a control analysis, we also examined signals from sensory networks (combining somatosensory, auditory, and visual regions) and computed their covariance with the FPCN or DMN (Fig. 3 *D*–*I*). Given no specific predictions for individual sensory networks, we collapsed all three sensory regions into a single network (see *SI Appendix* and *SI Appendix*, Fig. S4 for network selection). Of note, results were similar when evaluating each sensory network alone (*SI Appendix*).

As predicted, SCZ patients exhibited significantly higher FPCN–DMN covariance compared with HCS [$t(273) = 4.31$, $P < 3 \times 10^{-5}$, Cohen's $d = 0.48$] (Fig. 3 *A* and *B*). Again, BD patients did not differ from matched HCS in FPCN–DMN covariance [$t(124) = 0.063$, $P = 0.95$, n.s.] (Fig. 3*C*). We statistically confirmed the preferentially increased FPCN–DMN covariance in SCZ across all three groups (one-way ANOVA, SCZ, HCS, and BD) [$F(1, 451) = 12.09$, $P < 8 \times 10^{-6}$]. We also found elevated FPCN-sensory covariance in SCZ compared with HCS [$t(292) = 3.87$, $P = 0.00013$, Cohen's $d = 0.43$] (Fig. 3 *D* and *E*), but not in BD patients compared with HCS [$t(95) = 0.39$, $P = 0.69$] (Fig. 3*D*). In contrast, DMN-sensory covariance (Fig. 3 *G*–*I*) did not differ significantly between SCZ and matched HCS [$t(306) = 1.15$, $P = 0.25$] or between BD and matched HCS [$t(102) = 1.4$, $P = 0.18$], suggesting preferential changes in the FPCN between-network connectivity in SCZ. FPCN between-network connectivity effects were not driven by smoking status or movement (*SI Appendix*, Fig. S1 *E*–*I*). We again identified a relationship between FPCN–DMN connectivity effects and medication dose (*SI Appendix*, Fig. S1*D*), however effects were not explained by medication in a subset of BD patients that received antipsychotics (*SI Appendix*, Fig. S10*A*). As before, we verified that effects were not driven by global signal removal ($P = 0.0033$) (*SI Appendix*, Fig. S2). Collectively, these results indicate that FPCN GBC and its functional

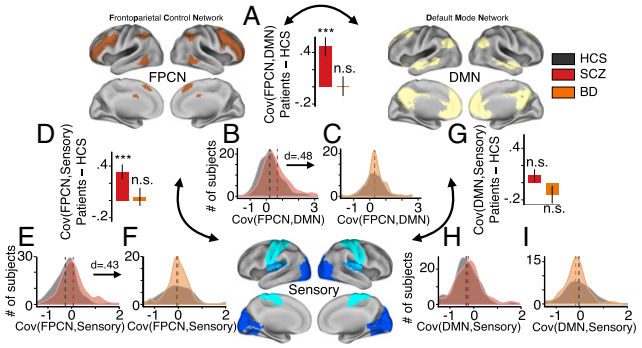

Fig. 3. FPCN between-network functional connectivity is preferentially increased in SCZ. Between-network connectivity was computed for the FPCN (*Upper Left*), DMN (*Upper Right*), and the sensory networks (*Lower*, combining somatosensory, auditory, and visual networks), using the average BOLD signal from each network. Bar plots highlight the group difference (patients–HCS) for each between-network connectivity measure: (*A*) FPCN-DMN connectivity group difference for SCZ–HCS (red) and BD–HCS (orange). (*B* and *C*) Distribution of FPCN–DMN connectivity values for each group (SCZ, red; HCS, black/gray; BD, orange), confirming specificity in SCZ. (*D*) FPCN-sensory connectivity group difference for SCZ–HCS and BD–HCS. (*E* and *F*) Distribution of FPCN-sensory connectivity values for each group, confirming specificity in SCZ. (*G*) DMN-sensory connectivity group difference for SCZ–HCS and BD–HCS. (*H* and *I*) Distribution of DMN-sensory connectivity values, revealing no effects in either clinical group. Error bars mark ±1 SE of the difference of means. ***$P < 0.001$; Cov, covariance; n.s., not significant; *d*, Cohen's *d* effect size. Vertical dashed lines represent group mean values.

connectivity with other networks are preferentially altered in SCZ, in line with hypotheses raised by prior work (22).

Next, we examined the possible clinical relevance of altered FPCN–DMN connectivity. We specifically focused on positive SCZ symptoms given prior reports suggesting that these effects may relate to psychosis severity (22). We identified a modest, but significant positive relationship between positive SCZ symptoms and the magnitude of observed FPCN–DMN covariance (r = 0.18, P = 0.03), suggesting clinical relevance of this effect (*SI Appendix*, Fig. S5).

Understanding Inhomogeneously Elevated Functional Connectivity in SCZ via Computational Modeling. As mentioned, initial whole-brain data-driven analyses (Fig. 1*H*) revealed elevated GBC in SCZ compared with HCS, localized to association regions, especially the FPCN (Fig. 2), which also displayed preferentially altered between-network connectivity in SCZ (Fig. 3). However, the initial homogeneous architecture of our model, by definition, could not explain this preferential association network effect. That is, because all nodes used the same physiological parameters, the model did not incorporate network inhomogeneity, and could not produce observed clinical network effects.

We hypothesized that SCZ effects could be captured through implementation of biologically plausible inhomogeneity in local recurrent self-excitation across the model architecture, based on anatomical and physiological evidence for hierarchical differences in cortical dynamics (*Discussion*). Put differently, we hypothesized that a widespread disruption in cortical E/I balance in SCZ may yield emergent preferential network dysconnectivity effects because of greater vulnerability of higher-order "association" circuits, arising from their distinct patterns of recurrence (34, 39, 40).

To test this theory, we divided the 66-node model into two distinct networks: "nonassociation" (or "sensory") nodes with lower recurrent excitation, and "association" nodes with higher recurrent excitation (*SI Appendix*) (Fig. 4*A*). This functional separation was informed by a biologically grounded observation: association cortex neuronal populations generally exhibit greater local recurrent excitation (39, 40, 44) compared with those in lower-order sensory cortex. In turn, we recalibrated model parameters for the E and I pools of all nodes in the differentiated model to achieve E/I balance (a mean firing rate of ∼3 Hz at each E pool). This was implemented to achieve appropriate balance for the different coexisting effective E-E weights of association and nonassociation nodes, producing the initial "healthy" regime. We assigned each node to a network (association vs. nonassociation) based on their unique anatomical location and connections using the interareal anatomical connectivity derived from human diffusion-weighted imaging, as validated in prior work (18) (*Experimental Procedures* and *SI Appendix*).

As before, we perturbed E/I balance by manipulating the described key model parameters from healthy baseline values toward elevated E/I. However, instead of using a uniform scalar multiplier (w) for E-E weight, we instead implemented network-specific values for w. Specifically, w_A (for the association network nodes) was three-times greater than w_S (for sensory nodes), guided by empirical studies (*SI Appendix*) (34, 39, 40). Thus, we could vary the weight of local recurrent excitation (E-E weight) for the differentiated model, while explicitly maintaining proportionately distinct recurrence properties in association vs. nonassociation network nodes (Fig. 4*A*).

Using model-derived BOLD signals (66 total), we computed within-network connectivity, similar to GBC, except restricted to association and sensory networks (*SI Appendix*). As before, we manipulated E/I ratio by varying four key model parameters: E-E weight (Fig. 4*B*), E-I weight (Fig. 4*C*), G (Fig. 4*D*), and σ (Fig. 4*E*). Consistent with SCZ effects, we found that within-network connectivity preferentially increased for association relative to

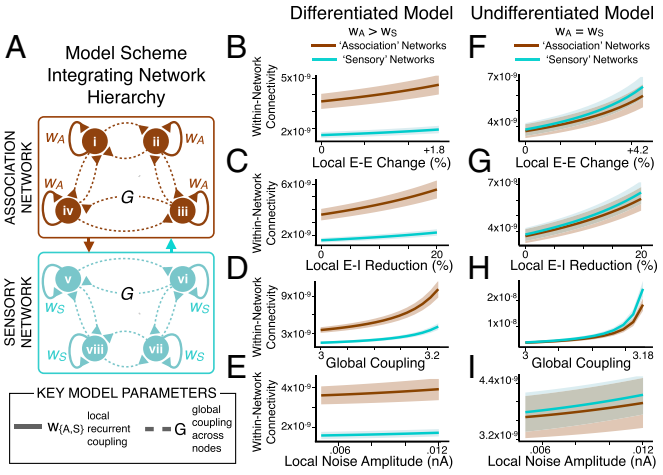

Fig. 4. Preferential network-level connectivity changes emerge from a functional hierarchy. (*A*) Differentiated model scheme, illustrating association (brown) versus sensory (cyan) nodes in the model with network-specific scalar multiplier values ($w_A > w_S$) for recurrent local self-excitation (E-E weight). Illustration depicts 8 nodes for visual simplicity, but full model has 66 nodes, divided into 38 association and 28 nonassociation (sensory) nodes based on anatomical connectivity. BOLD signals were extracted from each node of the model. We perturbed E/I ratio by varying four key model parameters: recurrent local self-excitation (E-E weight) within nodes, local recurrent inhibition (E-I weight) within nodes, long-range global coupling (G) between nodes, and local noise amplitude (σ) within all nodes. (*B–E*). Mean within-network connectivity (mean covariance of each node in a network with all other nodes in the same network, for either association or sensory nodes) (*SI Appendix*) was computed for the differentiated model ($w_A > w_S$) as a function of increasing E/I via increasing E-E weight, reducing E-I weight, increasing G, or increasing σ. Within-network connectivity preferentially increased in association nodes as E/I imbalance became more severe. Shading represents the SD of within-network connectivity values as evaluated for four separate simulations with different starting random noise. (*F–I*) Undifferentiated model results, using homogeneous values of recurrent local excitation (E-E weight) via a uniform scalar multiplier value ($w_A = w_S$) for E-E weight at all nodes. Here we define association and sensory nodes by their distinct anatomical connectivity (rather than any functional difference in recurrent excitation). In contrast to the differentiated model, anatomical connectivity differences alone could not account for preferential effects in association regions (also see *SI Appendix*, Fig. S6). Within-network connectivity values are in arbitrary units.

sensory nodes as a function of disinhibition via E-E weight, E-I weight, or G (Fig. 4 *B–D*, brown vs. cyan, and Fig. 5 *A–C*, showing increasing difference between association vs. sensory node values).

As predicted, increasing unshared variance in the signal (via σ, local noise amplitude) (Fig. 4*E*) did not contribute appreciably to within-network connectivity elevation in the model. Critically, these network differences were not evident for the undifferentiated model (Fig. 4 *F–I*, brown vs. cyan), despite preserving explicit differences in anatomical connectivity between the association and sensory nodes (*SI Appendix*, Fig. S6). Thus, the differential vulnerability to elevated E/I exhibited by the association vs. nonassociation nodes arose predominantly from functional differences in recurrent local excitation ($w_A > w_S$, specifically $w_A = 3 \times w_S$), and not from differences in anatomical connectivity profiles for association vs. sensory nodes (Fig. 4 *F–I*). Collectively, this neurobiologically grounded model expansion revealed that a system with different pre-existing network vulnerabilities could yield emergent preferential functional connectivity effects from a nonspecific global perturbation of E/I balance.

Connectivity Increases in SCZ Show Network-Dependent Patterns Consistent with Functional Hierarchy. Presented modeling results, in line with recent qualitative empirical reports (22), suggest a

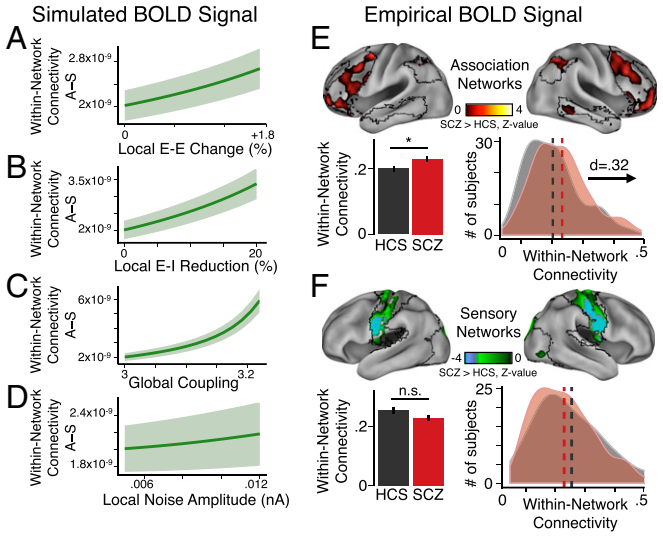

Fig. 5. Preferential network-level functional connectivity changes in SCZ follow modeling predictions. (*A–D*) Difference between association ("A") and sensory network ("S") within-network connectivity (as shown in Fig. 4), highlighting that within-network connectivity in A grows more steeply than in S as E/I elevation becomes more severe as a function of changing E-E weight, E-I weight, or *G*, but not σ. Shading represents the SD of values for the difference, A − S, in within-network connectivity evaluated across nodes for four separate simulations with different starting random noise. (*E*, *Upper*) Within-network connectivity group difference *z*-map shown across three major association networks: DMN, FPCN, and VAN (type I error corrected) (*SI Appendix*). (*Lower Left*) Group average for SCZ illustrates significantly elevated within-network connectivity in association networks compared with HCS. (*Lower Right*) Group distributions of mean within-network connectivity in association networks (SCZ, red; HCS, black/gray). (*F*, *Upper*) Within-network connectivity group difference *z*-map shown across three major sensory networks: somatosensory, auditory, and visual (type I error corrected) (*SI Appendix*). Group averages (*Lower Left*) and distributions (*Lower Right*) for SCZ and HCS reveal no significant differences for sensory networks. Error bars mark ±1 SEM; $*P < 0.05$. n.s., not significant; *d*, Cohen's *d* effect size. Vertical dashed lines represent the group mean values. Within-network connectivity in the model is in arbitrary units. Of note, here we focused our empirical analyses on a subset of carefully movement-matched subjects ($n = 130$ per group).

preferential vulnerability for association networks compared with lower-order sensory networks in SCZ. Next, we tested this preferential prediction in SCZ across combined association networks compared with sensory networks. Specifically, we averaged within-network connectivity values across three large-scale association networks, the FPCN, DMN, and VAN (Fig. 5*E*), extending our initial focused network characterization (Fig. 3). The key reason for combining association or sensory networks was to achieve an appropriate match between the model and empirical data (see *SI Appendix* for network matching between experiment and model). Given that our voxel-wise within-network connectivity analysis inevitably involves spatially adjacent voxels, which are vulnerable to head movement artifact, we focused our analyses (Fig. 5 *E* and *F*) on movement-matched subsets of 130 SCZ and 130 HCS.

As predicted by the model, we found elevated within-network connectivity across association regions in SCZ compared with HCS [$t(254) = 2.55$, $P < 0.015$, Cohen's $d = 0.32$] (Fig. 5*E*). In contrast, sensory within-network connectivity revealed no significant difference between movement-matched SCZ and HCS (Fig. 5*F*). This was further verified via a significant *Group* × *Network* interaction [two-way ANOVA for SCZ vs. HCS, association vs. sensory networks, $F(1, 258) = 19.90$, $P = 1.22 \times 10^{-5}$]. This effect was again specific to SCZ; there was no significant *Group* effect or *Group* × *Network* interaction for BD vs. HCS [two-way ANOVA for BD vs. HCS, association vs. sensory networks, $F(1, 127) = 0.428$, $P = 0.51$] (*SI Appendix*, Fig. S7 *C* and *D*). BD patients did not display significantly different head movement profiles from matched HCS ($P = 0.41$). Furthermore, magnitude of head motion was negatively correlated with the identified association network covariance (*SI Appendix*, Fig. S8), an effect completely inconsistent with the possibility that head motion spuriously drove elevated covariance in SCZ. Collectively, these empirical effects are in line with predictions of the functionally differentiated model. This finding suggests that higher-order association networks may be preferentially disrupted in SCZ, despite a common putative cellular-level disturbance across the cortex (20, 29).

Variance Increases in SCZ Show Preferential Network Patterns Consistent with Functional Hierarchy. Above, we examined measures of within- and between-network connectivity for association and sensory networks. Our connectivity measure (GBC) is based upon the mean covariance between a single region and the rest of the brain. This does not include the variance of the region itself. Although the maximum covariance necessarily places a lower bound on the variance of each region, there could be important differences in the BOLD signal variance between SCZ and HCS, as implicated in previous studies (18, 59). We therefore repeated our analysis, replacing the GBC with local variance, finding comparable results.

Using the identical model architecture, we computed the variance of BOLD signals for association and sensory nodes as a function of increasing E/I via four key parameters (Fig. 6 *B–E*). BOLD signal variance preferentially increased for association relative to sensory nodes as a function of increasing E/I (Fig. 6 *B–E*, brown vs. cyan, and Fig. 7 *A–D*, showing difference of association–sensory measures). Again, these preferential effects were absent in the undifferentiated model (Fig. 6 *F–I*, brown vs. cyan), suggesting that differences in recurrent local self-excitation (implemented by setting network-specific scalar multipliers of E-E weights: $w_A > w_S$) drove these effects, rather than differences in anatomical connectivity. Critically, these additional model-generated effects extend predictions to another functional measure, namely BOLD signal variance, previously implicated in SCZ (18, 59). Consequences of functional differentiation on model baseline activity are presented in *SI Appendix*, Fig. S13.

In turn, we empirically tested for preferentially elevated variance in association networks in SCZ, quantifying, for each subject, the mean voxel-wise variance within association networks (defined using the DMN, FPCN, and VAN). In line with model predictions under increased E/I (Fig. 6 *B–E*), we found elevated average BOLD signal variance for association networks in SCZ compared with HCS [$t(273) = 4.32$, $P < 2.2 \times 10^{-5}$, Cohen's $d = 0.48$] (*SI Appendix*, Fig. S9*A*). We observed more modest effects in sensory networks [$t(255) = 3.52$, $P < 0.0006$, Cohen's $d = 0.39$] (*SI Appendix*, Fig. S9*B*). However, preferential association network findings were confirmed statistically [two-way ANOVA, $F(1, 323) = 6.94$, $P = 0.009$].

As noted, movement artifacts can significantly affect BOLD signal, especially variance (60), in spatially specific ways. Therefore, we repeated all analyses using movement-matched samples (Fig. 7*E*), which also revealed elevated BOLD signal variance in association regions in SCZ compared with HCS [$t(258) = 2.42$, $P < 0.02$, Cohen's $d = 0.30$] (Fig. 7*E*, *Lower Left*). Here we observed no effects for sensory networks (Fig. 7*F*), highlighting preferential association effects [confirmed again via a *Group* × *Network* interaction; two-way ANOVA, $F(1, 258) = 9.54$, $P = 0.0022$ for the movement-matched sample]. To visualize effects, we generated voxel-wise variance maps, which illustrate elevated association (Fig. 7*E*) vs. sensory network variance (Fig. 7*F*). Collectively, these empirical effects are in line with model-generated predictions.

A key aspect of the model-generated results indicates that the same functional parameter, namely elevated E/I, can affect both association cortex variance and functional connectivity. Put

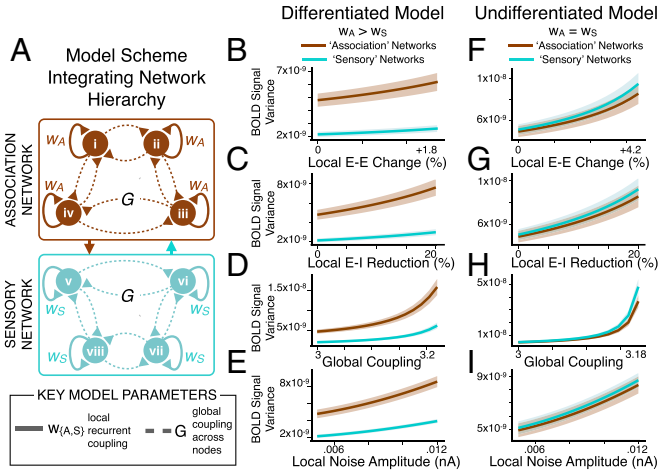

Fig. 6. Preferential network-level variance changes emerge from a functional hierarchy. (*A*) Model schematic. Illustration depicts eight nodes for simplicity; full model uses 66 nodes. (*B–E*) Mean BOLD signal variance of association or sensory nodes as a function of increasing E-E weight (*B*), percent reduction of E-I weight (*C*), *G* (*D*), or σ (*E*), showing that variance preferentially increases for association nodes as E/I elevation becomes more severe. Shading represents the SD of variance values as evaluated for four separate simulations with different starting random noise. (*F–I*) Undifferentiated model ($w_A = w_S$) results, using homogeneous values of local recurrent excitation at all nodes. As before, undifferentiated association and sensory nodes are defined by their distinct anatomical connectivity (rather than any functional difference in recurrent excitation). In contrast to the differentiated model, anatomical connectivity differences alone could not account for observed in vivo effects. BOLD signal variance in the model is in arbitrary units.

differently, the model predicts the two measures should be highly correlated. To test this, we related association cortex variance and connectivity across all subjects (*SI Appendix*, Fig. S12). As predicted, empirical results revealed a significant positive relationship across both HCS and SCZ movement-matched samples [r(Pearson) = 0.49, $P < 2.0 \times 10^{-17}$; r(Spearman) = 0.56, $P < 2.2 \times 10^{-16}$, $n = 260$].

Model Quantification. Above, we have qualitatively compared the undifferentiated and differentiated models on their ability to reproduce empirical effects. Specifically, the differentiated model produced preferential association effects, whereas the undifferentiated model did not. We formally quantified these distinct predictions (Fig. 8) by projecting model results into a 4D space. We represented four key dependent measures: association within-network connectivity change, sensory within-network connectivity change, association variance, and sensory variance. A lower-dimensional illustration is shown in Fig. 8*A*. Next, we computed the cosine similarity between model predictions and empirically observed differences (changes) in SCZ compared with HCS (Fig. 8 *B–E*). Finally, we randomly permuted the network assignments (association vs. nonassociation) for all model nodes across 1,000 iterations to establish the cosine similarity expected by chance between the models and the empirical data. Next, we computed the difference in cosine similarity for the differentiated (inhomogeneous) vs. the undifferentiated (homogeneous) model (Fig. 8 *F–I*; see *SI Appendix* for details). This analysis revealed that the (unpermuted) differentiated model significantly outperforms the undifferentiated model at reproducing empirical effects.

Discussion

Complex mental illnesses such as SCZ are associated with abnormal interactions between cortical regions (61), particularly association and prefrontal cortices (22). However, studies examining SCZ repeatedly implicate disturbances across distributed cortical territories, including primary visual (62, 63) and auditory circuits (64–66). Therefore, there exists a tension between findings implicating focal disruptions within higher-order association cortices (2, 3, 9, 31) and cellular-level hypotheses, suggesting widespread synaptic alterations, supported by pharmacological and preclinical studies (20, 62). We combined computational modeling and clinical neuroimaging in an attempt to link levels of analysis, from a hypothesized widespread cellular-level neuropathology in SCZ (20, 21) to preferential neural network disruption identified via neuroimaging. First, the modeling simulations predicted preferential effects of E/I imbalance in association regions, which were not explained by structural connectivity differences alone. Second, key modeling predictions were confirmed empirically in SCZ across a number of neuroimaging measures, which were unremarkable in a control sample of BD patients. These computational and empirical effects collectively support a parsimonious theoretical account that helps to reconcile the tension between emergent preferential disruptions of association networks in the context of globally elevated cortical E/I in SCZ.

Focal vs. Global Neuropathology Producing Preferential Association Deficits in SCZ. SCZ is characterized by profound cognitive deficits (16), associated with disturbances in association regions, particularly those involving executive processing, which relies on prefrontal cortex (PFC) function (67, 68). There is now strong converging neuroimaging evidence implicating disturbances in the PFC and other association regions in SCZ (18, 22, 24, 69, 70), with corresponding thalamo-cortical dysconnectivity (25, 26). Additional evidence suggests SCZ effects are broadly distributed; it is associated with abnormal belief formation, hallucinations,

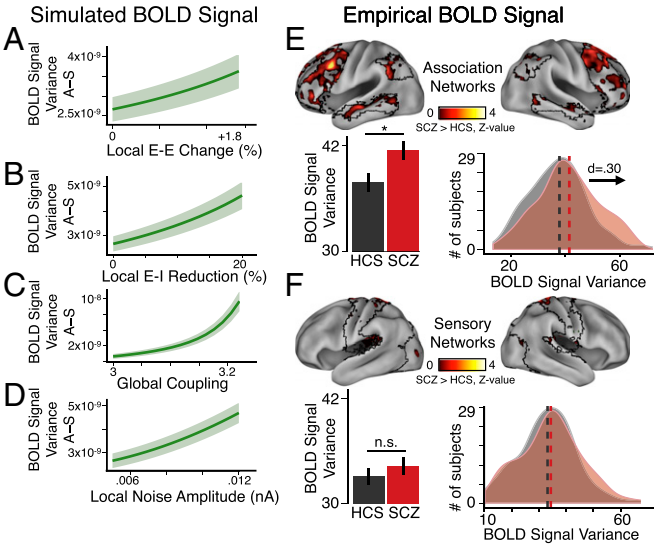

Fig. 7. Preferential network-level variance changes in SCZ follow modeling predictions. (*A–D*) Difference in variance between the association ("A") and sensory nodes ("S") (similar to Fig. 5). (*E*, *Upper*) We computed a between-group voxel-wise BOLD signal variance *z*-map restricted to association network regions (specifically DMN, FPCN, and VAN) (type I error corrected) (*SI Appendix*). (*Lower*) Group averages and distributions illustrate elevated variance for association networks in SCZ compared with matched HCS. (*F*) Analyses for the sensory networks show no significant effects. We focused empirical analyses on a subset of movement-matched subjects, given the possibility that BOLD signal variance is particularly susceptible to head motion (102). Nevertheless, all reported association cortex effects held in the full sample (*SI Appendix*, Fig. S9 *A* and *B*). Error bars mark ± 1 SEM; *$P < 0.05$. n.s., not significant; *d*, Cohen's *d* effect size. Vertical dashed lines represent the group mean values. Model variance is in arbitrary units.

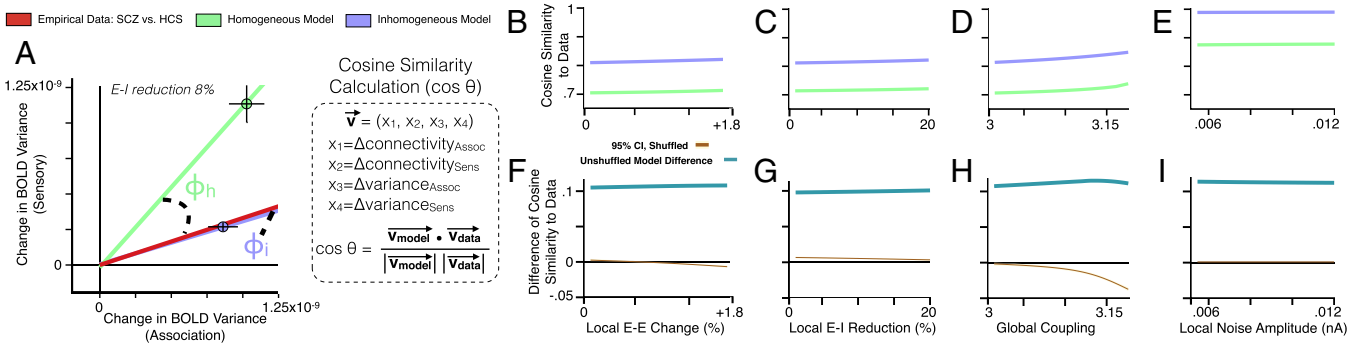

Fig. 8. Quantitative model comparison. We used four measures to assess models and empirical data: (*i*) within-network connectivity in association regions, (*ii*) within-network connectivity in sensory regions, (*iii*) BOLD signal variance in association regions, and (*iv*) BOLD signal variance in sensory regions. (*A*) Change in measures 3–4 on the *x* and *y* axis, respectively. The green and blue dots represent the amount of change in each measure when the models (homogeneous and inhomogeneous) are pushed toward elevated E/I ratio via an 8% reduction in E-I weight relative to the healthy starting values. Of note, other E-I reductions (we simulated from 0% up to 20%) all fall closely along the same vectors for each model regime. Because the magnitudes of the model vectors are in arbitrary units, we focused on quantifying the angle of the model vector formed by elevations in E/I, rather than the magnitude. Specifically, we computed the angle between the model vector and the data vector (φ_h for the homogeneous model, φ_i for the inhomogeneous model). The data vector (red) is computed by subtracting mean values for HCS in each measure from the mean values for SCZ on the same measure, to obtain a change in measure, exactly as done for the model data. The red line represents the direction of the vector formed by the empirical data. Formula box: We projected both model simulations and empirical data into a 4D space analogous to the 2D example in *A*, using the four dependent measures (x_1–x_4) as axes in the 4D space (x_1 = change in within-network connectivity in association regions, x_2 = change in within-network connectivity in sensory regions, x_3 = change in BOLD signal variance in association regions, and x_4 = change in BOLD signal variance in sensory regions). The angle θ between the model and the empirical data were used to compute the cosine similarity (cos θ) between these vectors, with 1 representing perfect similarity between vectors. (*B*–*E*) Cosine similarity values, for the similarity between respective model simulations and empirical data, were computed for both the homogeneous ($\cos\theta_h$) and inhomogeneous ($\cos\theta_i$) models, as a function of increasing E/I along four parameters: increasing E-E weight (*B*), reducing E-I weight (*C*), increasing global coupling (*D*), or increasing local noise amplitude (*E*). (*F*–*I*) Plots of the difference between models with respect to their cosine similarity to the empirical data ($\cos\theta_i - \cos\theta_h$). The teal line represents the values computed for the models as a function of increasing E/I ratio from baseline. After generating 1,000 random permutations of the node identities (association vs. nonassociation) for both models, we recomputed the difference of cosine similarity to empirical data ($\cos\theta_i - \cos\theta_h$), to estimate the values expected by chance. The brown line represents the mean difference of cosine similarity expected by chance. The 95% confidence interval (yellow shading) around the brown line is barely visible because of minimal spread of the distribution.

anhedonia, and deficits in primary sensory processing (71–76). Indeed, many studies reveal abnormalities in lower-order sensory perception (62) and auditory gating deficits in SCZ (77–79), suggesting more widespread neural disturbances. Thus, competing hypotheses of SCZ include focal alterations in higher-order networks versus a more general neural dysfunction affecting widespread cortical territories.

In parallel, evidence from postmortem SCZ studies reveals disrupted expression of genes involved in synaptic excitation and inhibition in the PFC (8, 9, 27, 80, 81). Other studies implicate localized reductions in dendritic spine density (2), potentially impacting regional recurrent self-excitation dynamics in SCZ. Such studies have yet to be repeated across the cortical mantle to test whether these deficits could impact E/I balance across cortical circuits in SCZ. Consistent with this possibility, pharmacological models of SCZ often propose a distributed disruption in E/I across cortical circuits. This finding is supported by clinical magnetic resonance spectroscopy studies showing GABA and glutamate deficits across the cortex in SCZ (7, 82–84).

In summary, empirical evidence exists both for global and localized hypotheses of neuropathology in SCZ. It may be possible to unify these hypotheses by considering normal differences in functional properties of cortical circuits that span the information-processing hierarchy in the brain. We present evidence suggesting that a globally homogeneous disinhibition can produce preferential effects in association regions as a consequence of pre-existing differences in physiological properties for association vs. nonassociation regions. Importantly, the globally altered E/I hypothesis is consistent with the data. However, our data do not necessarily rule out potential alternative hypotheses of more region-specific phenomena, which may co-occur or perhaps emerge more selectively in some patient subgroups. It is ultimately an empirical question if all SCZ symptoms stem from a global disturbance or from regionally specific pathology. The key advance here is in showing that a global model of elevated E/I is capable of reproducing network-preferential findings. Future studies should use more quantitative predictions allowing for rigorous evaluation of "global" vs. "regional" model perturbations. Ideally, this would be done after fitting models to empirical data using dynamic causal modeling methods (85).

Reconciling Preferential Connectivity Changes in Association Cortex in the Context of a Distributed Microcircuit Neuropathology in SCZ. Emerging findings (38, 39) support a hierarchy of information processing across the primate cortical mantle. This provides a parsimonious and neurobiologically grounded assumption that can be readily integrated into existing computational models of resting-state activity (18, 42, 43). Put differently, hierarchically linked functional differences across brain regions may lead to differences in vulnerability to homogeneously distributed E/I imbalance. Here we tested for emergent preferential network disruptions in SCZ by considering neurobiologically plausible functional differences across the cortical hierarchy in our model. We specifically focused on recurrent excitation, which differs across sensory and association regions.

This implementation of functional hierarchy in the model is based on multiple anatomical and physiological findings in primates. Anatomically, cortical pyramidal cells display significant regional variation in dendritic morphology. In particular, both the number and density of dendritic spines per neuron increases along the cortical hierarchy (34, 36, 37). Consequently, pyramidal cells in association areas can receive more excitatory inputs per neuron than those in lower-level sensory areas. This property may correspond physiologically to an increase in local recurrent excitation strength at higher levels of the information-processing hierarchy. Indeed, computational models suggest that hierarchical differences in local recurrent excitation strength underlie differences in the neural activity time-scales observed across

cortical regions in primates, and consequently may support specialization across cortical areas (39, 40, 44). Collectively, these basic neuroscience findings motivated our in silico implementation of different recurrent local excitation properties for association relative to sensory nodes.

This parsimonious assumption produced preferential effects in the model's association regions for all investigated measures. Critically, emergent network effects were not simply a consequence of different interareal anatomical connectivity in association nodes (*SI Appendix*, Fig. S6). Preferential association network effects did not emerge in the undifferentiated model, which assumed homogenous local recurrent excitation but maintained differences in interareal anatomical connectivity across networks (Figs. 4 and 6). We verified all model predictions empirically, confirming preferential association cortex effects for all measures, which were in turn positively related, as predicted by the model (*SI Appendix*, Fig. S12). These convergent findings suggest that more severe association network deficits in SCZ may emerge from normal microcircuit properties that give rise to differential recurrent dynamics in association regions. Put simply, association networks may be more vulnerable to E/I imbalance thought to occur in SCZ. Notably, the model suggests elevated E/I in the resting-state condition. Importantly, the cortical regime in resting state might be different from the regime during task engagement, thus present findings may be compatible with reduced recurrent excitatory strength during cognitive processing (86).

The Interplay of Biophysically Based Computational Modeling and Psychiatric Neuroimaging. This study establishes an example of the interplay between computational modeling and experimental clinical neuroimaging, in line with recent proposals for a computational psychiatry framework (29, 45). Our starting point was a homogenous, undifferentiated model using a well-established computational framework (18, 42, 43). This model architecture generated the initial experimental prediction for cortical hyperconnectivity tested here in chronic SCZ patients (Fig. 1). However, data-driven clinical analyses revealed preferential network-level alterations. This directly motivated the model architecture expansion whereby we incorporated neurobiologically plausible mechanisms for hierarchical specialization of cortical microcircuitry (34, 38–40, 44). Although parsimonious in its implementation, this differentiated model generated additional key experimental predictions that arose uniquely from its emergent large-scale neural dynamics. For example, the model strongly predicted that elevated E/I could preferentially affect both association cortex variance and functional connectivity. This prediction was confirmed (Figs. 5 and 7, and *SI Appendix*, Fig. S12), illustrating the interplay between the model and experimental effects. The ability of biophysically based computational models to generate predictions across levels of experimental analysis (29, 45, 87) is especially critical for computational psychiatry applications in severe disorders, such as SCZ, which affect multiple interconnected pathways at the local circuit and systems levels. Collectively, this study establishes a proof-of-principle computational psychiatry approach whereby neurobiologically grounded modeling of clinical data can generate results that help explain multiple distinct clinical neuroimaging effects.

Considering Preferential Diagnostic Findings. Initially, one might argue that analyzing 5 min of rs-fMRI data does not really inform (cellular or synaptic) pathophysiology. For example, there could be differences between two groups of people who are told they are being scanned because they are healthy controls or because there is something wrong with their brain. However, these deflationary explanations cannot explain why the SCZ group showed the selective dissociation in terms of functional connectivity within association and sensory networks but the bipolar group did not. We aimed to identify a potential mechanism underlying observed neuroimaging effects of SCZ, as opposed to an effect that may occur across many neuropsychiatric diagnoses. As noted, none of the SCZ effects were observed in our independent BD sample. Thus, SCZ effects may reflect an underlying neuropathology that unique to this clinical population. This theory is supported by the identified relationship between FPCN–DMN connectivity and positive SCZ symptom severity (*SI Appendix*, Fig. S5). Future investigations should examine if some SCZ effects might be shared among BD patients that also present with co-occurring psychosis (22) or similar functional connectivity profiles (22, 25, 88). This represents an important opportunity for future computational psychiatry studies that extend models of neuropsychiatric disease to explain symptoms cross-diagnostically (89).

Implications for Treatment Development. It is therapeutically relevant to determine whether SCZ arises from a global disruption, with preferential network-level effects, or alternatively stems from regionally localized disruptions. Antipsychotic medications predominantly target dopaminergic and serotonergic signaling in the striatum (90–92) and are effective for treating psychosis. In contrast, the devastating cognitive deficits in SCZ may relate to abnormal glutamatergic signaling (93, 94) upstream of the dopaminergic dysregulation (5). Our simulations have further shown that distinct patterns of recurrence can impact severity of E/I imbalance effects across regions. Consequently, this may necessitate fine-tuned glutamateric treatments for functionally distinct cortical areas. It will be critical for future studies to explore such treatment considerations. Computational studies that simulate translational therapies and the effect of such "compensations" on the network disruptions may therefore inform rationally guided therapeutic design for psychiatric illness.

Broader Clinical Implications. Present results, showing that regional differences in recurrent excitation can produce differential vulnerability to disinhibition, have several broader implications. First, pharmacological neuroimaging agents may impact neural E/I balance. Thus, it may be necessary to characterize effects of these agents on a network-by-network basis because of variations in recurrent dynamics. Second, our findings suggest key considerations for neurodevelopmental studies. For example, changes in synaptic density and cortical gray matter volume occur during maturation (95), with the association cortex undergoing gray matter volume loss only at the end of adolescence, coinciding with peak age of SCZ onset. Furthermore, SCZ and NMDAR hypofunction disturbances have similar age-dependency profiles: administering NMDAR antagonists in high doses triggers psychotic symptoms in adults but not children (96). Our findings suggest that ordinary developmental changes in the association cortex could alter local recurrent dynamics and consequently alter vulnerability to NMDAR-mediated changes in E/I. Indeed, studies support the link between elevated recurrent excitation in association regions and their increased NMDAR/AMPAR ratio (97). These findings may link evolving dynamical properties of the developing brain and the age-dependency of SCZ onset.

Limitations. Our modeling and clinical effects need to be considered with some important caveats. First, the current model still maintains a cortico-centric architecture and does not incorporate subcortical pathways (98). Although the current architecture generated predictions for cortical network effects in SCZ, incorporating cortico-striatal-thalamic loops will be critical for future studies to allow testing of subcortical mechanisms, especially "functional neurotransmitter loops" incorporating effects of dopamine and other neurotransmitters not explored in our model (additional discussion in *SI Appendix*). As noted, some of the presented effects were correlated with medication dose at the

time of the scan. This may reflect disease severity (as more symptomatic patients typically receive higher antipsychotic doses). Of note, our observations of BD patients receiving atypical antipsychotics did not suggest a medication confound (*SI Appendix*, Fig. S10). Nevertheless, studies in medication-naïve patients will be vital. Also, it is important to consider that our simulations assumed no structural differences between groups and instead generated predictions based on functional parameters. Given possible interareal anatomical connectivity alteration in chronic SCZ patients (99), future work that uses whole-brain probabilistic tractography approaches (100) will be key to generate appropriate modeling constraints across groups to improve model fits.

Conclusion. This study addresses an explanatory gap between observations of widespread cellular pathology and preferential network-level neuroimaging abnormalities in SCZ. Our biophysical simulations of elevated E/I predicted increased functional connectivity in SCZ. This was confirmed empirically in SCZ, but appeared to preferentially impact association regions. To capture these observations, we integrated regional functional differences into the model; this produced preferential functional connectivity and variance disruptions in association regions in the model under elevated E/I, which we confirmed empirically in SCZ patients. Collectively, our findings advance a parsimonious mechanism bridging preferential network-level disruptions in SCZ with a potentially global pathology. In doing so, we present a framework for hierarchical functional disturbance in SCZ, which may help to inform future treatment and neuroimaging biomarker refinement.

Experimental Procedures

Participants. Here we studied two independent clinical samples: (*i*) 161 chronic SCZ patients and 164 demographically matched HCS (*SI Appendix*, Table S1) recruited from the Olin Neuropsychiatry Research Center and from a publicly distributed dataset provided by the Center for Biomedical Research Excellence (fcon_1000.projects.nitrc.org/indi/retro/cobre.html); and (*ii*) 73 patients diagnosed with BD and 56 HCS also recruited from the Olin Neuropsychiatry Research Center (25) (*SI Appendix*, Table S2). Across samples, all subjects met identical neuroimaging exclusion criteria, underwent identical preprocessing, quality assurance, and analyses (see *SI Appendix* for full recruitment details). Across all samples we accomplished matching on a number of relevant variables, ensuring comparable between-group demographics. For additional comprehensive procedures regarding subject selection, inclusion/exclusion criteria, group matching, medication, and symptom analyses, please see *SI Appendix*.

Neuroimaging Methods. For a full description of neuroimaging acquisition, preprocessing and analysis details please see *SI Appendix*.

Computational Modeling. We used a validated computational model of resting-state functional connectivity (18, 42, 43), extending a local circuit model (46) to coupled large-scale networks. The 66 nodes of our model are each composed of separate excitatory (E) and inhibitory (I) pools, representing local excitatory and inhibitory neurons. The E pools are coupled through an interareal anatomical connectivity matrix, derived from diffusion tractography in humans (48). The inhibition strengths of the I pools vary by node to maintain a uniform baseline firing rate in E cells (~3 Hz). Our current model closely follows the feedback inhibition control model reported by Deco et al. (42), except that we also include a globally shared noise component corresponding to empirically observed global signals (GS) in resting-state fMRI studies (18). Complete modeling details are presented in the *SI Appendix*.

ACKNOWLEDGMENTS. Financial support was provided by National Institutes of Health Grants DP50D012109-02 [to A.A., PI (principal investigator)], MH080912 (to D.C.G., PI), and MH43775, MH077945, and MH074797 (to G.D.P., PI); National Institute on Alcohol Abuse and Alcoholism Grant 2P50AA012870-11 (to J.H.K., PI); the National Alliance for Research on Schizophrenia and Depression Young Investigator award (to A.A., PI); Grant R01-MH062349 (to X-J.W. and J.D.M.); National Institutes of Health Grant T32GM 007205 (to G.J.Y.); National Institute of Neurological Disorders and Stroke Grant T32 NS007224 (to G.J.Y.); and the Yale Center for Clinical Investigation (A.A., PI).

1. Garey L (2010) When cortical development goes wrong: Schizophrenia as a neurodevelopmental disease of microcircuits. *J Anat* 217(4):324–333.
2. Glantz LA, Lewis DA (2000) Decreased dendritic spine density on prefrontal cortical pyramidal neurons in schizophrenia. *Arch Gen Psychiatry* 57(1):65–73.
3. Kolluri N, Sun Z, Sampson AR, Lewis DA (2005) Lamina-specific reductions in dendritic spine density in the prefrontal cortex of subjects with schizophrenia. *Am J Psychiatry* 162(6):1200–1202.
4. Carlsson M, Carlsson A (1990) Schizophrenia: A subcortical neurotransmitter imbalance syndrome? *Schizophr Bull* 16(3):425–432.
5. Coyle JT (2006) Glutamate and schizophrenia: Beyond the dopamine hypothesis. *Cell Mol Neurobiol* 26(4-6):365–384.
6. Matthysse S, Lipinski J (1975) Biochemical aspects of schizophrenia. *Annu Rev Med* 26:551–565.
7. Poels EM, et al. (2014) Glutamatergic abnormalities in schizophrenia: A review of proton MRS findings. *Schizophr Res* 152(2-3):325–332.
8. Dracheva S, et al. (2001) N-methyl-D-aspartic acid receptor expression in the dorsolateral prefrontal cortex of elderly patients with schizophrenia. *Am J Psychiatry* 158(9):1400–1410.
9. Hashimoto T, et al. (2003) Gene expression deficits in a subclass of GABA neurons in the prefrontal cortex of subjects with schizophrenia. *J Neurosci* 23(15):6315–6326.
10. Krystal JH, State MW (2014) Psychiatric disorders: Diagnosis to therapy. *Cell* 157(1): 201–214.
11. Schizophrenia Working Group of the Psychiatric Genomics Consortium (2014) Biological insights from 108 schizophrenia-associated genetic loci. *Nature* 511(7510): 421–427.
12. Kehrer C, Maziashvili N, Dugladze T, Gloveli T (2008) Altered excitatory-inhibitory balance in the NMDA-hypofunction model of schizophrenia. *Front Mol Neurosci* 1:6.
13. Javitt DC (1987) Negative schizophrenic symptomatology and the PCP (phencyclidine) model of schizophrenia. *Hillside J Clin Psychiatry* 9(1):12–35.
14. Tandon R (2013) Schizophrenia and other psychotic disorders in DSM-5. *Clin Schizophr Relat Psychoses* 7(1):16–19.
15. Weickert TW, et al. (2000) Cognitive impairments in patients with schizophrenia displaying preserved and compromised intellect. *Arch Gen Psychiatry* 57(9):907–913.
16. Barch DM, Ceaser A (2012) Cognition in schizophrenia: Core psychological and neural mechanisms. *Trends Cogn Sci* 16(1):27–34.
17. Javitt DC (2009) When doors of perception close: Bottom-up models of disrupted cognition in schizophrenia. *Annu Rev Clin Psychol* 5:249–275.
18. Yang GJ, et al. (2014) Altered global brain signal in schizophrenia. *Proc Natl Acad Sci USA* 111(20):7438–7443.
19. Jardri R, Denève S (2013) Circular inferences in schizophrenia. *Brain* 136(Pt 11): 3227–3241.
20. Krystal JH, et al. (2003) NMDA receptor antagonist effects, cortical glutamatergic function, and schizophrenia: Toward a paradigm shift in medication development. *Psychopharmacology (Berl)* 169(3-4):215–233.
21. Schobel SA, et al. (2013) Imaging patients with psychosis and a mouse model establishes a spreading pattern of hippocampal dysfunction and implicates glutamate as a driver. *Neuron* 78(1):81–93.
22. Baker JT, et al. (2014) Disruption of cortical association networks in schizophrenia and psychotic bipolar disorder. *JAMA Psychiatry* 71(2):109–118.
23. Bastos-Leite AJ, et al. (2015) Dysconnectivity within the default mode in first-episode schizophrenia: A stochastic dynamic causal modeling study with functional magnetic resonance imaging. *Schizophr Bull* 41(1):144–153.
24. Whitfield-Gabrieli S, et al. (2009) Hyperactivity and hyperconnectivity of the default network in schizophrenia and in first-degree relatives of persons with schizophrenia. *Proc Natl Acad Sci USA* 106(4):1279–1284.
25. Anticevic A, et al. (2014) Characterizing thalamo-cortical disturbances in schizophrenia and bipolar illness. *Cereb Cortex* 24(12):3116–3130.
26. Woodward ND, Karbasforoushan H, Heckers S (2012) Thalamocortical dysconnectivity in schizophrenia. *Am J Psychiatry* 169(10):1092–1099.
27. Hashimoto T, et al. (2008) Conserved regional patterns of GABA-related transcript expression in the neocortex of subjects with schizophrenia. *Am J Psychiatry* 165(4): 479–489.
28. Marín O (2012) Interneuron dysfunction in psychiatric disorders. *Nat Rev Neurosci* 13(2):107–120.
29. Anticevic A, et al. (2013) Connectivity, pharmacology, and computation: Toward a mechanistic understanding of neural system dysfunction in schizophrenia. *Front Psychiatry* 4(169):169.
30. Palaniyappan L, Simmonite M, White TP, Liddle EB, Liddle PF (2013) Neural primacy of the salience processing system in schizophrenia. *Neuron* 79(4):814–828.
31. Lewis DA (2000) Is there a neuropathology of schizophrenia? Recent findings converge on altered thalamic-prefrontal cortical connectivity. *Neuroscientist* 6(3): 208–218.
32. Friston KJ (1996) Theoretical neurobiology and schizophrenia. *Br Med Bull* 52(3): 644–655.
33. Volkow ND, et al. (1988) Brain interactions in chronic schizophrenics under resting and activation conditions. *Schizophr Res* 1(1):47–53.
34. Elston GN (2003) Cortex, cognition and the cell: New insights into the pyramidal neuron and prefrontal function. *Cereb Cortex* 13(11):1124–1138.

35. Elston GN, Rosa MG, Calford MB (1996) Comparison of dendritic fields of layer III pyramidal neurons in striate and extrastriate visual areas of the marmoset: A Lucifer yellow intracellular injection. *Cereb Cortex* 6(6):807–813.
36. Elston GN, Tweedale R, Rosa MG (1999) Cortical integration in the visual system of the macaque monkey: Large-scale morphological differences in the pyramidal neurons in the occipital, parietal and temporal lobes. *Proc Biol Sci* 266(1426): 1367–1374.
37. Elston GN, Tweedale R, Rosa MG (1999) Cellular heterogeneity in cerebral cortex: A study of the morphology of pyramidal neurones in visual areas of the marmoset monkey. *J Comp Neurol* 415(1):33–51.
38. Scholtens LH, Schmidt R, de Reus MA, van den Heuvel MP (2014) Linking macroscale graph analytical organization to microscale neuroarchitectonics in the macaque connectome. *J Neurosci* 34(36):12192–12205.
39. Murray JD, et al. (2014) A hierarchy of intrinsic timescales across primate cortex. *Nat Neurosci* 17(12):1661–1663.
40. Chaudhuri R, Knoblauch K, Gariel MA, Kennedy H, Wang XJ (2015) A large-scale circuit mechanism for hierarchical dynamical processing in the primate cortex. *Neuron* 88(2):419–431.
41. Anticevic A, et al. (2012) NMDA receptor function in large-scale anticorrelated neural systems with implications for cognition and schizophrenia. *Proc Natl Acad Sci USA* 109(41):16720–16725.
42. Deco G, et al. (2014) How local excitation-inhibition ratio impacts the whole brain dynamics. *J Neurosci* 34(23):7886–7898.
43. Deco G, et al. (2013) Resting-state functional connectivity emerges from structurally and dynamically shaped slow linear fluctuations. *J Neurosci* 33(27):11239–11252.
44. Wang XJ (2001) Synaptic reverberation underlying mnemonic persistent activity. *Trends Neurosci* 24(8):455–463.
45. Wang XJ, Krystal JH (2014) Computational psychiatry. *Neuron* 84(3):638–654.
46. Wong KF, Wang XJ (2006) A recurrent network mechanism of time integration in perceptual decisions. *J Neurosci* 26(4):1314–1328.
47. Friston KJ, Mechelli A, Turner R, Price CJ (2000) Nonlinear responses in fMRI: The Balloon model, Volterra kernels, and other hemodynamics. *Neuroimage* 12(4): 466–477.
48. Hagmann P, et al. (2008) Mapping the structural core of human cerebral cortex. *PLoS Biol* 6(7):e159.
49. Krystal JH, et al. (1994) Subanesthetic effects of the noncompetitive NMDA antagonist, ketamine, in humans. Psychotomimetic, perceptual, cognitive, and neuroendocrine responses. *Arch Gen Psychiatry* 51(3):199–214.
50. Mohn AR, Gainetdinov RR, Caron MG, Koller BH (1999) Mice with reduced NMDA receptor expression display behaviors related to schizophrenia. *Cell* 98(4):427–436.
51. Olney JW, Newcomer JW, Farber NB (1999) NMDA receptor hypofunction model of schizophrenia. *J Psychiatr Res* 33(6):523–533.
52. Cole MW, Anticevic A, Repovs G, Barch D (2011) Variable global dysconnectivity and individual differences in schizophrenia. *Biol Psychiatry* 70(1):43–50.
53. Cole MW, Yang GJ, Murray JD, Repovs G, Anticevic A (2015) Functional connectivity change as shared signal dynamics. *J Neurosci Methods* 259:22–39.
54. Beneyto M, Morris HM, Rovensky KC, Lewis DA (2012) Lamina- and cell-specific alterations in cortical somatostatin receptor 2 mRNA expression in schizophrenia. *Neuropharmacology* 62(3):1598–1605.
55. Hoftman GD, et al. (2015) Altered cortical expression of GABA-related genes in schizophrenia: Illness progression vs developmental disturbance. *Schizophr Bull* 41(1):180–191.
56. Lewis DA, Hashimoto T (2007) Deciphering the disease process of schizophrenia: The contribution of cortical GABA neurons. *Int Rev Neurobiol* 78:109–131.
57. Lewis DA, Hashimoto T, Volk DW (2005) Cortical inhibitory neurons and schizophrenia. *Nat Rev Neurosci* 6(4):312–324.
58. Power JD, et al. (2011) Functional network organization of the human brain. *Neuron* 72(4):665–678.
59. Hahamy A, et al. (2014) Save the global: Global signal connectivity as a tool for studying clinical populations with functional magnetic resonance imaging. *Brain Connect* 4(6):395–403.
60. Kim J, Van Dijk KR, Libby A, Napadow V (2014) Frequency-dependent relationship between resting-state functional magnetic resonance imaging signal power and head motion is localized within distributed association networks. *Brain Connect* 4(1): 30–39.
61. Friston KJ, Frith CD (1995) Schizophrenia: A disconnection syndrome? *Clin Neurosci* 3(2):89–97.
62. Calderone DJ, et al. (2013) Comparison of psychophysical, electrophysiological, and fMRI assessment of visual contrast responses in patients with schizophrenia. *Neuroimage* 67:153–162.
63. Lencz T, et al. (2003) Impairments in perceptual competency and maintenance on a visual delayed match-to-sample test in first-episode schizophrenia. *Arch Gen Psychiatry* 60(3):238–243.
64. Hoffman RE, Fernandez T, Pittman B, Hampson M (2011) Elevated functional connectivity along a corticostriatal loop and the mechanism of auditory/verbal hallucinations in patients with schizophrenia. *Biol Psychiatry* 69(5):407–414.
65. Javitt DC, Strous RD, Grochowski S, Ritter W, Cowan N (1997) Impaired precision, but normal retention, of auditory sensory ("echoic") memory information in schizophrenia. *J Abnorm Psychol* 106(2):315–324.
66. Vercammen A, Knegtering H, den Boer JA, Liemburg EJ, Aleman A (2010) Auditory hallucinations in schizophrenia are associated with reduced functional connectivity of the temporo-parietal area. *Biol Psychiatry* 67(10):912–918.
67. Cole MW, Repovš G, Anticevic A (2014) The frontoparietal control system: A central role in mental health. *Neuroscientist* 20(6):652–664.
68. Pearlson GD, Petty RG, Ross CA, Tien AY (1996) Schizophrenia: A disease of heteromodal association cortex? *Neuropsychopharmacology* 14(1):1–17.
69. Gupta CN, et al. (2015) Patterns of gray matter abnormalities in schizophrenia based on an international mega-analysis. *Schizophr Bull* 41(5):1133–1142.
70. Radhu N, et al. (2015) Evidence for inhibitory deficits in the prefrontal cortex in schizophrenia. *Brain* 138(Pt 2):483–497.
71. Kay SR, Fiszbein A, Opler LA (1987) The positive and negative syndrome scale (PANSS) for schizophrenia. *Schizophr Bull* 13(2):261–276.
72. Berenbaum H, Oltmanns TF (1992) Emotional experience and expression in schizophrenia and depression. *J Abnorm Psychol* 101(1):37–44.
73. Kring AM, Kerr SL, Smith DA, Neale JM (1993) Flat affect in schizophrenia does not reflect diminished subjective experience of emotion. *J Abnorm Psychol* 102(4): 507–517.
74. Goldman-Rakic PS (1994) Working memory dysfunction in schizophrenia. *J Neuropsychiatry Clin Neurosci* 6(4):348–357.
75. Stephan KE, Friston KJ, Frith CD (2009) Dysconnection in schizophrenia: From abnormal synaptic plasticity to failures of self-monitoring. *Schizophr Bull* 35(3): 509–527.
76. Tek C, et al. (2002) Visual perceptual and working memory impairments in schizophrenia. *Arch Gen Psychiatry* 59(2):146–153.
77. Hamm JP, Gilmore CS, Picchetti NA, Sponheim SR, Clementz BA (2011) Abnormalities of neuronal oscillations and temporal integration to low- and high-frequency auditory stimulation in schizophrenia. *Biol Psychiatry* 69(10):989–996.
78. Kwon JS, et al. (1999) Gamma frequency-range abnormalities to auditory stimulation in schizophrenia. *Arch Gen Psychiatry* 56(11):1001–1005.
79. Tsuchimoto R, et al. (2011) Reduced high and low frequency gamma synchronization in patients with chronic schizophrenia. *Schizophr Res* 133(1-3):99–105.
80. Akbarian S, et al. (1996) Selective alterations in gene expression for NMDA receptor subunits in prefrontal cortex of schizophrenics. *J Neurosci* 16(1):19–30.
81. Maldonado-Avilés JG, et al. (2009) Altered markers of tonic inhibition in the dorsolateral prefrontal cortex of subjects with schizophrenia. *Am J Psychiatry* 166(4): 450–459.
82. Marsman A, et al. (2014) GABA and glutamate in schizophrenia: A 7 T ^{1}H-MRS study. *Neuroimage Clin* 6:398–407.
83. Marsman A, et al. (2013) Glutamate in schizophrenia: A focused review and meta-analysis of ^{1}H-MRS studies. *Schizophr Bull* 39(1):120–129.
84. Taylor SF, Tso IF (2015) GABA abnormalities in schizophrenia: A methodological review of in vivo studies. *Schizophr Res* 167(1-3):84–90.
85. Kahan J, et al. (2014) Resting state functional MRI in Parkinson's disease: The impact of deep brain stimulation on 'effective' connectivity. *Brain* 137(Pt 4):1130–1144.
86. Wang M, et al. (2013) NMDA receptors subserve persistent neuronal firing during working memory in dorsolateral prefrontal cortex. *Neuron* 77(4):736–749.
87. Murray JD, et al. (2014) Linking microcircuit dysfunction to cognitive impairment: effects of disinhibition associated with schizophrenia in a cortical working memory model. *Cereb Cortex* 24(4):859–872.
88. Anticevic A, et al. (2015) Ventral anterior cingulate connectivity distinguished nonpsychotic bipolar illness from psychotic bipolar disorder and schizophrenia. *Schizophr Bull* 41(1):133–143.
89. Cuthbert BN, Insel TR (2010) Toward new approaches to psychotic disorders: The NIMH Research Domain Criteria project. *Schizophr Bull* 36(6):1061–1062.
90. Andrade C, Kharawala S (2007) First- vs second-generation antipsychotic drugs in schizophrenia. *Arch Gen Psychiatry* 64(8):978–979, author reply 979–980.
91. Davis JM, Chen N, Glick ID (2003) A meta-analysis of the efficacy of second-generation antipsychotics. *Arch Gen Psychiatry* 60(6):553–564.
92. Kane JM, et al. (1998) Guidelines for depot antipsychotic treatment in schizophrenia. European Neuropsychopharmacology Consensus Conference in Siena, Italy. *Eur Neuropsychopharmacol* 8(1):55–66.
93. Dunlop J, Brandon NJ (2015) Schizophrenia drug discovery and development in an evolving era: Are new drug targets fulfilling expectations? *J Psychopharmacol* 29(2): 230–238.
94. Walker AG, Conn PJ (2015) Group I and group II metabotropic glutamate receptor allosteric modulators as novel potential antipsychotics. *Curr Opin Pharmacol* 20: 40–45.
95. Rakhade SN, Jensen FE (2009) Epileptogenesis in the immature brain: Emerging mechanisms. *Nat Rev Neurol* 5(7):380–391.
96. Reich DL, Silvay G (1989) Ketamine: An update on the first twenty-five years of clinical experience. *Can J Anaesth* 36(2):186–197.
97. Lisman JE, Fellous JM, Wang XJ (1998) A role for NMDA-receptor channels in working memory. *Nat Neurosci* 1(4):273–275.
98. Lisman J (2012) Excitation, inhibition, local oscillations, or large-scale loops: What causes the symptoms of schizophrenia? *Curr Opin Neurobiol* 22(3):537–544.
99. Griffa A, et al. (2015) Characterizing the connectome in schizophrenia with diffusion spectrum imaging. *Hum Brain Mapp* 36(1):354–366.
100. Sotiropoulos SN, et al.; WU-Minn HCP Consortium (2013) Advances in diffusion MRI acquisition and processing in the Human Connectome Project. *Neuroimage* 80: 125–143.
101. Cole MW, et al. (2013) Multi-task connectivity reveals flexible hubs for adaptive task control. *Nat Neurosci* 16(9):1348–1355.
102. Power JD, Barnes KA, Snyder AZ, Schlaggar BL, Petersen SE (2012) Spurious but systematic correlations in functional connectivity MRI networks arise from subject motion. *Neuroimage* 59(3):2142–2154.